THE JOURNAL OF BIOLOGICAL CHEMISTRY Vol. 275, No. 26, Issue of June 30, pp. 19877–19882, 2000
Printed in U.S.A.

Biophysical Characterization of gp41 Aggregates Suggests a Model for the Molecular Mechanism of HIV-associated Neurological Damage and Dementia*

Received for publication, February 7, 2000, and in revised form, March 10, 2000
Published, JBC Papers in Press, March 19, 2000, DOI 10.1074/jbc.M001036200

Michael Caffrey‡§, Demetrios T. Braddock‡§¶, John M. Louis‡§, Mones A. Abu-Asab¶, Douglas Kingma¶, Lance Liotta¶, Maria Tsokos¶, Nancy Tresser‖, Lewis K. Pannell, Norman Watts‡‡, Alasdair C. Steven‡‡, Martha N. Simon§§, Stephen J. Stahl¶¶, Paul T. Wingfield¶¶, and G. Marius Clore‡‖‖**

*From the ‡Laboratory of Chemical Physics, NIDDK, National Institutes of Health, Bethesda, Maryland 20892-0510, the ¶Laboratory of Pathology, NCI, National Institutes of Health, Bethesda, Maryland 20892, ‖Neuroimmunology Branch, NINDS, National Institutes of Health, Bethesda, Maryland 20892, the **Laboratory of Bioorganic Chemistry, NIDDK, National Institutes of Health, Bethesda, Maryland 20892, the ‡‡Laboratory of Structural Biology Research, NIAMS, National Institutes of Health, Bethesda, Maryland 20892, the §§Department of Biology, Brookhaven National Laboratory, Upton, New York 11973-5000, and the ¶¶Protein Expression Laboratory, NIAMS, National Institutes of Health, Bethesda, Maryland 20892*

In human immunodeficiency virus (HIV)-infected individuals, the level of the HIV envelope protein gp41 in brain tissue is correlated with neurological damage and dementia. In this paper we show by biochemical methods and electron microscopy that the extracellular ectodomain of purified HIV and simian immunodeficiency virus gp41 (e-gp41) forms a mixture of soluble high molecular weight aggregate and native trimer at physiological pH. The e-gp41 aggregate is shown to be largely α-helical and relatively stable to denaturants. The high molecular weight form of e-gp41 is variable in size ranging from 7 to 70 trimers, which associate by interactions at the interior of the aggregate involving the loop that connects the N- and C-terminal helices of the e-gp41 core. The trimers are predominantly arranged with their long axes oriented radially, and the width of the high molecular weight aggregate corresponds to the length of two e-gp41 trimers (~200 Å). Using both light and electron microscopy combined with immunohistochemistry we show that HIV gp41 accumulates as an extracellular aggregate in the brains of HIV-infected patients diagnosed with dementia. We postulate that the high molecular weight aggregates of e-gp41 are responsible for HIV-associated neurological damage and dementia, consistent with known mechanisms of encephalopathy.

Up to 80% of HIV[1]-infected individuals suffer neurological damage, and of these ~20% are afflicted with HIV-associated dementia (HAD) (1, 2). HIV infection does not result in the productive infection of neurons (3–6), and consequently indirect mechanisms for the pathogenesis of HAD have been proposed (7, 8). The elaboration of neurotoxic agents following HIV infection have supported this notion (9), and recent work has shown that levels of the HIV envelope protein gp41 in the brain are correlated with the severity and rate of progression of HAD (10–13). The underlying mechanism, however, for the damaging neurological effects of gp41 is currently unknown.

The biochemical properties of the ectodomains of HIV and SIV gp41 (e-gp41) are relatively well characterized (14–18). Recombinant HIV and SIV e-gp41 produced in *Escherichia coli* forms insoluble precipitates at neutral pH (14, 18), and solubilization can be accomplished by either reducing the pH to less than 4 (18) or by deleting the long loop that connects the N- and C-terminal helices of the ectodomain core (14). The helical core of the HIV and SIV e-gp41 is extremely resistant to denaturation and proteolysis (14, 18), the structure of the complete ectodomain of SIV gp41 has been solved by NMR spectroscopy (19), and structures of the helical core of HIV and SIV e-gp41 have been solved by x-ray crystallography (20–24). In the present paper, we correlate the biochemical behavior and EM appearance of HIV and SIV e-gp41 with the neuropathology observed in patients diagnosed with HAD. The present study suggests that the accumulation of a highly stable, high molecular weight form of the HIV gp41 ectodomain in the brains of HIV-infected individuals may provide a rational explanation for the origin of HIV-associated neurological damage and dementia, which is consistent with known mechanisms of encephalopathy.

MATERIALS AND METHODS

Biochemical Analysis of e-gp41—The HIV and SIV e-gp41 constructs employed are those described in Ref. 18, specifically residues 27–154 for HIV (strain HXB2) gp41 and residues 27–149 for SIV (strain Mac239) gp41 (using the numbering scheme from Ref. 18). Size exclusion chromatography of e-gp41 (200–300 μg) under various experimental conditions of buffer, pH, and denaturant (urea or guanidinium chloride) was carried out on a Superdex-200 column (1 × 30 cm; Amersham Pharma-

* This work was supported by the Intramural AIDS Targeted Antiviral Program of the Office of the Director of the National Institutes of Health (to G. M. C., P. T. W., and A. C. S.). The Brookhaven National Laboratory STEM is a National Institutes of Health supported Resource Center (NIH P41-RR-1777) with additional support provided by Department of Energy, Office of Biological and Environmental Research. The costs of publication of this article were defrayed in part by the payment of page charges. This article must therefore be hereby marked "*advertisement*" in accordance with 18 U.S.C. Section 1734 solely to indicate this fact.

§ Contributed equally to this work.

‖‖ To whom correspondence should be addressed: Laboratory of Chemical Physics, Bldg. 5, Rm. B1-30I, NIDDK, National Institutes of Health, Bethesda, MD 20892-0510. Tel.: 301-496-0782; Fax: 301-496-0825; E-mail: clore@speck.niddk.nih.gov.

[1] The abbreviations used are: HIV, human immunodeficiency virus; HAD, HIV-associated dementia; SIV, simian immunodeficiency virus; e-gp41, ectodomain of gp41; EM, electron microscopy; CD, circular dichroism; STEM, scanning transmission electron microscopy; CTEM, conventional transmission electron microscopy.

cia Biotech) at a flow rate of 0.7 ml/min (Åkta explorer, Amersham Pharmacia Biotech). Protease reactions were performed in 100 μl of 0.1 M $NaHCO_3$, pH 8.0, containing 30 μg of purified e-gp41 aggregate and 0.3 μg of trypsin for 1 h at 37 °C. CD spectra were recorded on a JASCO J-720 spectropolarimeter using a 0.01-cm path length cell and 23 μM protein (monomer units) in 0.1 M $NaHCO_3$, pH 8.0. Mass analysis of proteolytic digests was carried out by injecting protein (50–100 pmol) into a Zorbax C3 column (2.3 x 150 mm, Hewlett Packard, San Jose, CA) fitted to an HP1100 integrated high pressure liquid chromatography/electrospray mass spectrometer (Hewlett Packard) equilibrated in 5% acetic acid. The solvent was held isocratic for 25 min to allow desalting of the protein and then ramped to 100% acetonitrile over a period of 25 min at a flow rate of 200 μl/min. Protein peaks that eluted into the mass spectrometer were scanned from m/z 500 to 1700 every 4 s. Spectra were deconvoluted using the Hewlett Packard software to yield the mass of the protein.

EM Studies of e-gp41—Samples of SIV e-gp41 trimers or aggregate were examined by negative stain transmission EM. Samples (50 μg/ml) were applied to air glow-discharged carbon-coated grids and stained with 1% uranyl acetate. Micrographs were recorded at ×30,000 magnification with a Zeiss EM902 (Carl Zeiss, Thornwood, NY). Some samples were also stained with methylamine vanadate and examined by scanning transmission electron microscopy (STEM) (25). Mass determinations of e-gp41 aggregate particles were made from micrographs of freeze-dried specimens obtained at the Brookhaven National Laboratory STEM facility (26). Briefly, specimens were applied to prewetted thin carbon films (2–3 mm thick) supported on holey thick carbon films on titanium grids. Specimens were then rinsed repeatedly with 20 mM ammonium acetate, blotted to a thin film between two pieces of filter paper, and plunged into liquid nitrogen slush. Specimens were freeze-dried by gradual warming to −80 °C under high vacuum and then transferred under vacuum to the STEM. Images were recorded at 40 keV and an electron dose of $\ll$1000 electrons/nm^2 at −150 °C to minimize radiation damage. Tobacco mosaic virus particles (131.4 kDa/nm) included in the preparations served as a mass standard, and mass determinations were done with the software described in Ref. 27.

Immunohistochemistry—The autopsy records of the National Institutes of Health from 1985 to 1998 were examined to identify appropriate material for a limited re-examination of the neuropatology of HAD. The histology and immunochemistry of brain lesions in HAD are well described, and therefore one case from each of the following groups was chosen: a patient with AIDS, clinical dementia, and histological evidence of HAD complex; a patient with AIDS but without clinical dementia and no histological evidence of HAD complex; and a patient without AIDS, clinical dementia, or histological evidence of HAD complex.

Tissue was fixed in 10% buffered formalin for two weeks, sectioned, and embedded in paraffin. Serial 5-μm sections of blocks from the deep white matter were cut, and representative sections were stained with hematoxylin-eosin and examined for histology consistent with HAD. Mouse monoclonal antibody to gp41 (gp41.1, Genetic systems, Seattle, Washington) was employed to screen brain sections for the presence of gp41 at a 1:200 dilution using a Ventana Medical Systems Gen II (Tuczon, AZ) for detection. Positive and negative controls on tonsilar lymphoid tissue from non-HIV-infected individuals were performed with L-26 (positive control) and gp41 (negative control) monoclonal antibodies.

For EM studies, tissue sections corresponding to histological lesions of HAD complex were removed from a paraffin block, deparaffinated in xylene, placed in absolute ethanol, and embedded in LR White (SPI, West Chester, PA). Ultrathin sections were mounted on 150 mesh-uncoated nickle grids. Grids were floated on blocking solution (phosphate-buffered saline, 0.1% Tween 20, 0.5% cold water fish gelatin) for 20 min, incubated for 1 h with the primary anti-gp41 antibody (as described above), rinsed in blocking buffer for 5 min, then incubated with gold-conjugated secondary antibody 20 nm in length (Ted Pella, Inc., Redding, CA), rinsed in phosphate-buffered saline, water, and air dried. Section were stained with uranyl acetate and examined with a Phillips CM10 electron microscope.

RESULTS

Size Exclusion Chromatography of e-gp41—At pH 2.5, size exclusion chromatography shows that both HIV and SIV e-gp41 elute as a single peak corresponding to the trimeric form solved by NMR spectroscopy (10) with a molecular mass of about 45 kDa (Fig. 1*A*). During the course of our biochemical

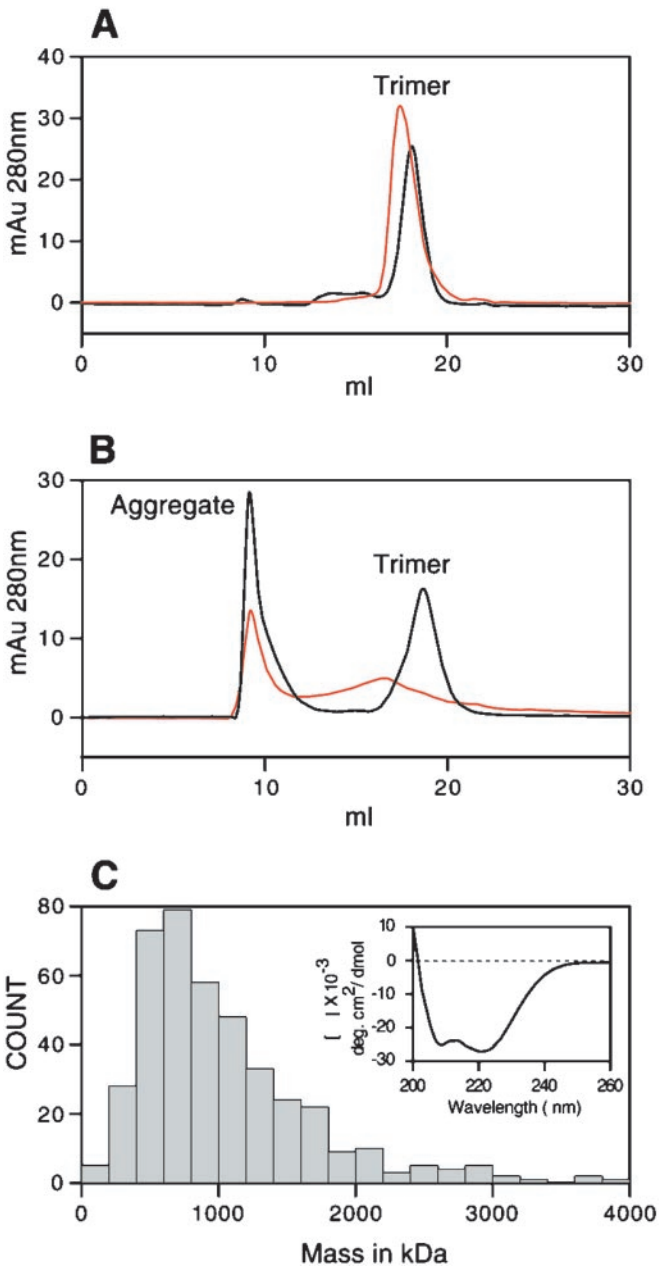

FIG. 1. **Characterization of the high molecular weight and trimeric forms of HIV and SIV gp41 ectodomains.** *A* and *B,* analysis of purified HIV (*red*) and SIV (*black*) gp41 ectodomains by size exclusion chromatography. gp41 ectodomain was fractionated on a Superdex-200 column in (*A*) 50 mM sodium formate, pH 2.5, and (*B*) 100 mM $NaHCO_3$, pH 8.0. *C,* histogram of masses observed for the purified high molecular weight form of SIV gp41 measured by STEM. The *inset* shows the CD spectrum of the purified high molecular weight form of SIV gp41.

characterization of HIV and SIV e-gp41 we noted that both nonglycosylated ectodomains are remarkably soluble with no visible precipitation in 0.1 M $NaHCO_3$ at pH 8. Under these conditions, both ectodomains elute as two forms, a high molecular weight form with an apparent molecular mass of about 600 kDa and the trimeric form (Fig. 1*B*). The proportion of the two forms can be altered by pH and urea. The trimeric form is favored at low pH, whereas the high molecular weight form is predominant at neutral pH. Both forms coexist about equally in 1 M urea. In 8 M urea, the ratio of high molecular weight to trimeric form is about 1:2 for the SIV e-gp41, and only the trimeric form is present in the case of the HIV e-gp41. Although the two forms are obviously in equilibrium, kinetic exchange

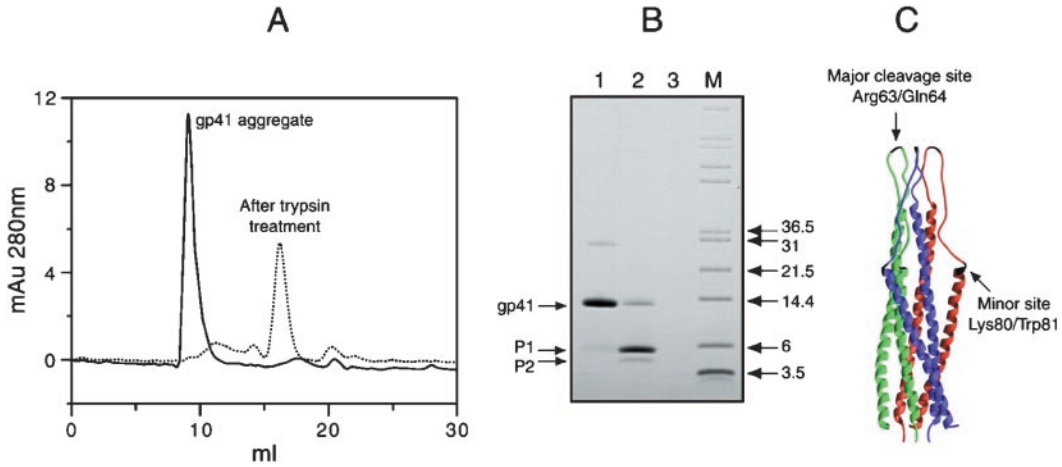

FIG. 2. **Digestion of the purified high molecular weight form of the ectodomain of SIV gp41 with trypsin and mapping of cleavage products.** Size-exclusion chromatography (*A*) and SDS-polyacrylamide gel electrophoresis (*B*) of the purified high molecular weight form before (*solid trace* and *lane 1*) and after (*dotted trace* and *lane 2*) digestion with trypsin. *C,* ribbon diagram of the trimeric SIV gp41 indicating the major ($Arg^{63} \downarrow Gln^{64}$) and minor ($Lys^{80} \downarrow Trp^{81}$) trypsin cleavage sites (shown in *black*). The coordinates are taken from Ref. 19 (PDB code 1QCE).

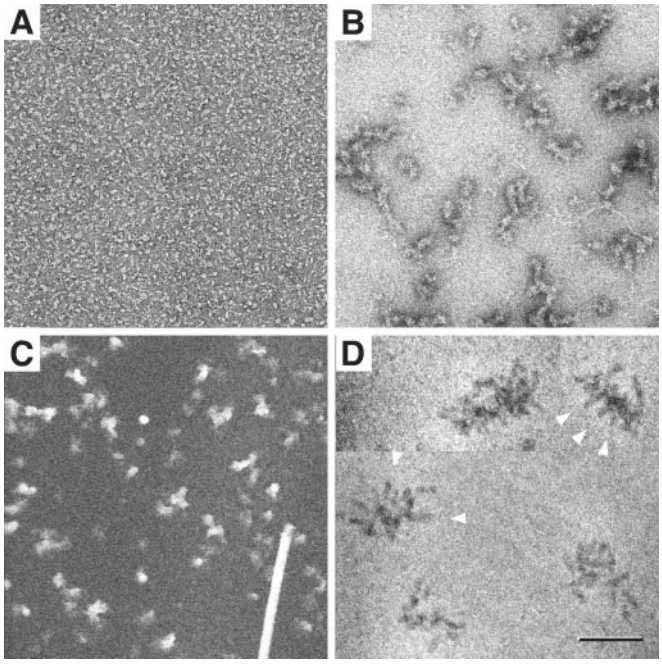

FIG. 3. **Electron microscopy of SIV e-gp41.** Displayed are CTEM images of trimeric protein (*A*) and high molecular weight aggregate (*B*) stained with uranyl acetate and unstained with high molecular weight aggregate used for STEM mass determinations (*C*), and a high magnification STEM view of the high molecular weight aggregate stained with vanadate (*D*). A tobacco mosaic virus particle used as an internal mass standard is visible in *C*. *Bar,* 100 nm in *A–C* and 25 nm in *D*. The *arrowheads* in *D* are directed at the finger-like protrusions.

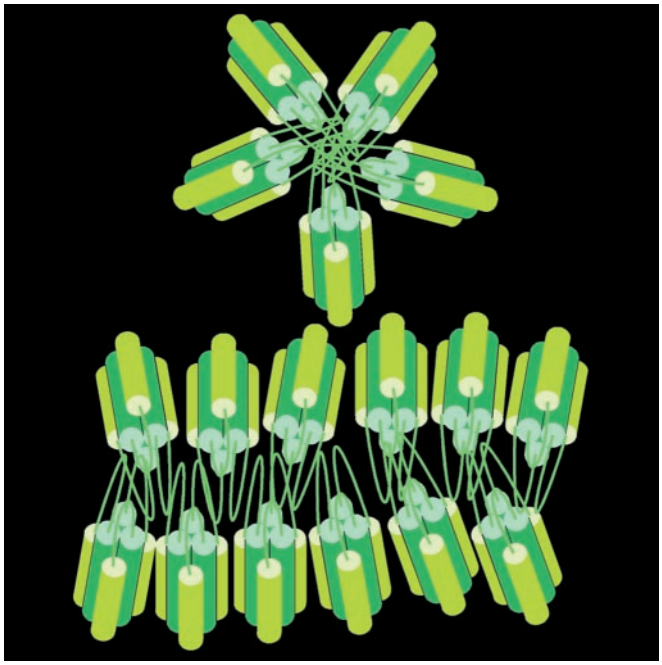

FIG. 4. **Model of the e-gp41 aggregate.** Trimers of the N- and C-terminal helices of e-gp41 associate radially via the connecting loops to form the high molecular weight aggregates. The model emphasizes the somewhat irregular nature of the association and the presence of both closed- and open-ended forms.

between the two forms is imperceptibly slow. Thus, the purified soluble high molecular weight form of SIV e-gp41 elutes as only a single peak on size-exclusion chromatography (Fig. 2*A*) and is stable for over a week.

Protease Digestion of the e-gp41 High Molecular Weight Aggregate—The CD spectrum of the high molecular weight form of SIV e-gp41 (Fig. 1*C, inset*) is characteristic of a highly helical structure and is essentially identical to that of the trimeric form (18). Thus, the tertiary structure remains unchanged upon formation of the high molecular weight form. To ascertain the mechanism of aggregation we subjected the purified high molecular weight form of SIV e-gp41 to trypsin digestion in 0.1 M $NaHCO_3$, pH 8. The elution profiles demonstrate that trypsin converts the high molecular weight form to the trimeric form (Fig. 2*A*). SDS-polyacrylamide gel electrophoresis shows that the full-length SIV e-gp41 (Fig. 2*B*, *lane 1*) is cleaved to a distinct smaller molecular weight product (*lane 2*, *band P1*) and a less distinct product (*lane 2, band P2*) that migrates just below the major product. The nearly equal intensity of the major band (*lane 2*, *band P1*) observed upon cleavage relative to that of the full-length polypeptide (*lane 1*) suggests that the two products of cleavage co-migrate in the same position. To confirm this observation and to map the sites of cleavage, a sample similar in composition to that in *lane 2* of Fig. 2*B* was subjected to liquid chromatography-electrospray mass spectrometry. Two distinct peaks with m/z 7235 and 7199 indicated one major cleavage site in the polypeptide spanning residues 1–63 and 64–123. This major cleavage site between Arg^{63} and Gln^{64} is located at the tip of the loop that connects the N- and C-terminal helices of the ectodomain core (Fig. 2*C*).

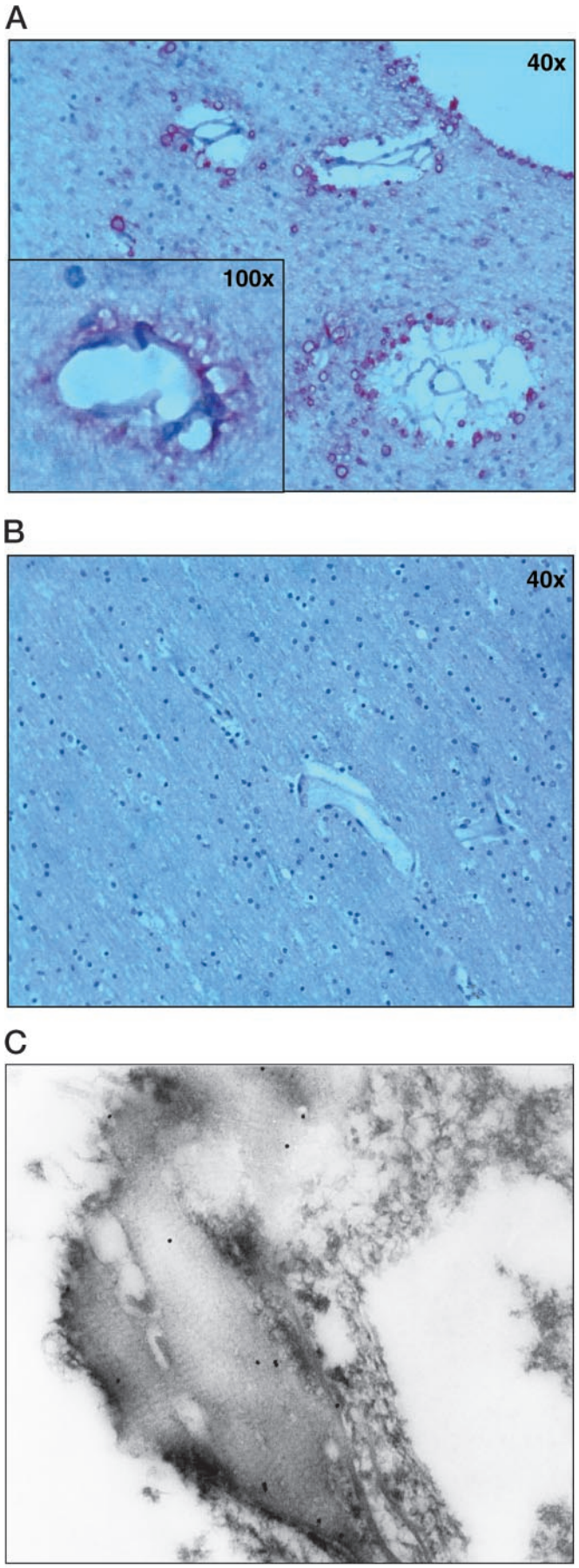

FIG. 5. Immunochemical staining of deep periventricular white matter using a monoclonal anti-HIV gp41 antibody from (*A*) an HAD-diagnosed individual and (*B*) an HIV-infected patient without histological or clinical evidence of HAD. Magnification in *A* and *B* is ×40 for the overall figures and ×100 for the *inset* in *A*. Numerous focal gp41 areas are observed (*purple*) in *A* and are particularly prominent around the vasculature. No such areas are seen in normal brains or in brains of HIV-infected individuals without HAD (*cf. B*). Indeed, the section in *B* depicts histologically normal brain parenchyma with no evidence of immunoperoxidase staining for gp41. *C,* electron micrograph at ×21,000 magnification. The brain tissue was incubated with a mouse monoclonal anti-gp41 antibody and detected with a gold-labeled secondary antibody. Areas of gp41 (seen as *black dots*) are localized in the extracellular collagen of the tunica adventitia of intraparenchymal capillaries. Negative controls showed no labeling with gold.

The minor P2 band (m/z 5369) corresponds to a secondary cleavage site between residues Lys^{80} and Trp^{81} of the C-terminal fragment (residues 64–123). This cleavage site is located at the N-terminal end of the C-terminal helix (Fig. 2*C*). The second product resulting from the minor cleavage was also detected with m/z 1847, corresponding to residues 64–80. These results suggest that the integrity of the loop that connects the N- and C-terminal helices of the ectodomain core is essential for e-gp41 aggregation. The same pattern of digestion was also observed with the HIV e-gp41 ectodomain as determined by SDS-polyacrylamide gel electrophoresis (data not shown).

Electron Microscopy of e-gp41 Aggregates—To further characterize the high molecular weight form of the gp41 ectodomain we carried out both conventional transmission electron microscopy (CTEM) and STEM. CTEM of negatively stained, purified high molecular weight form of gp41 (Fig. 3*B*) reveals aggregates that are heterogeneous in size and shape, although one dimension (the diameter in the case of globular particles, the width in the case of more elongated particles) is usually about 150–200 Å. In contrast, trimer preparations (Fig. 3*A*) show much smaller particles, including rodlets ~30 × 100 Å that are likely to represent side views of individual trimers. To some extent, the variability in appearance of the aggregates may represent different viewing angles. A quantitative measure of their heterogeneity is obtained from dark field STEM of unstained, freeze-dried specimens (Fig. 3*C*) (26, 27). In these digital micrographs, the number of scattered electrons in each pixel is directly proportional to the mass thickness. By summing over all pixels of an aggregate (and subtracting the substrate background), the mass of each aggregate can be determined, regardless of its orientation (26, 27). These data (Fig. 1*C*) show a broad distribution of masses ranging from ~300 kDa to >3000 kDa, peaking at ~ 650 kDa, with a mean of 1033 kDa. Because the experimental uncertainty in a single measurement for a particle of this molecular weight range is expected to be of the order of 2–5% (27), the heterogeneity is clearly real. It follows that the high molecular weight aggregates contain from ~7 to >70 trimers.

Dark field STEM micrographs of molecules embedded in a low density negative stain such as vanadate (25) provide a sensitive method for detecting fine details because maximum contrast in these images is achieved when the beam is optimally focused. With bright field CTEM, on the other hand, contrast is augmented by appropriate defocusing but at the expense of interference effects that may obscure fine details. A high magnification STEM micrograph of vanadate-stained gp41 aggregates is shown in Fig. 3*D*. Their dimensions are consistent with those in the CTEM (Fig. 3*B*). In these images, however, finger-like protrusions are frequently visible, extending at variable angles at the periphery of these particles (*e.g.* Fig. 3*D*, *arrowheads*). The width of these fingers is ~35Å, the diameter of a gp41 trimer.

Taken together the biochemical and EM observations imply that the aggregates consist of variable numbers (typically

7–70) of gp41 trimers, associated by means of interactions among their connecting loops at the interior of the aggregate. A model for the e-gp41 aggregate is presented in Fig. 4. The packing arrangement is not very regular, but the trimers are predominantly oriented with their long axes oriented radially, a property that explains the finger-like protuberances, as well as the characteristic dimension of 150–200 Å as two molecular lengths.

Immunohistochemistry of Brain Tissue in HAD—The severity and degree of dementia in HAD has been correlated to total gp41 levels in the brain, as determined using protein immunoblots (10, 11), and to the extent of gp41 immunostaining in brain slices (12). HAD, however, is not correlated to the levels of other HIV viral proteins (10) or to the viral load itself (28–34). The unique ability of e-gp41 to form stable high molecular weight aggregates provides an explanation for the longevity and immunogenicity of gp41 over other HIV proteins. In addition, extracellular aggregates of e-gp41 would be phagocytosed by brain macrophages and possibly astrocytes and would have the potential to induce the elaboration of cytokines as has been documented by several laboratories (35–37).

We therefore propose that the neurotoxicity of gp41 is related to the biophysical properties of e-gp41, namely its ability to self-associate into folded, stable, high molecular weight aggregates. The histological appearance of the high molecular weight form of gp41 would be difficult to observe by standard methods. For example, Congo Red staining, which stains β amyloid, would not be expected to stain a helical polymer. However, routine immunohistochemistry can highlight the presence of gp41 and has the ability to distinguish between membranous and nonmembranous protein localization. Immunostaining of brain sections in patients with HAD reveals numerous gp41 positive perivascular macrophages (Fig. 5*A*), confirming previous observations (12, 13, 38). In addition, the staining pattern is strongly suggestive of extracellular gp41 (*inset* in Fig. 5*A*). In contrast no evidence of immunoperoxidase staining for gp41 is observed in sections of brains from patients without HAD (Fig. 5*B*). The presence of extracellular gp41 in the brains of HAD individuals was confirmed by EM combined with histoimmunochemistry using a gold-labeled secondary antibody that clearly localizes gp41 to sites such as adventitial (perivascular) collagen (Fig. 5*C*).

Extracellular gp41 visualized by immunohistochemistry of HAD brains may represent extracellular viral particles or free aggregates of gp41. Because the severity and extent of HAD is correlated with gp41 and not viral load, it is very likely that the visualized extracellular gp41 represents high molecular weight aggregates of e-gp41.

DISCUSSION

At present there is no known explanation for gp41 neurotoxicity that results in HIV-associated neurological damage and dementia. Our biochemical results clearly demonstrate that HIV and SIV e-gp41 forms high molecular weight aggregates at physiological pH. Whereas the core of HIV and SIV e-gp41 is resistant to proteolysis and denaturation (14, 18), the regions N- and C-terminal to the ectodomain are sensitive to proteolysis. These observations lead us to speculate that in HIV-infected patients e-gp41 accumulates in the brain as a stable extracellular aggregate. We therefore propose the following molecular model for the role of gp41 in neurological damage and dementia. In the native state, e-gp41 is present on the exterior of both virus particles and infected cells and is anchored to the membrane by its C-terminal transmembrane region. The action of proteolytic enzymes within the brain could readily result in the release of e-gp41 into the extracellular matrix. Because of the biochemical properties of e-gp41, it would then form a high molecular weight aggregate at physiological pH, and it is the accumulation of these high molecular weight aggregates that lead to neurological damage and the subsequent clinical findings of dementia.

If aggregation of e-gp41 is responsible for HAD, one would expect to find histologic similarities between cerebral HIV lesions and cerebral lesions induced by other protein deposition disorders. Indeed, a spongiform encephalopathy morphologically indistinguishable from Creutzfeldt-Jakob disease has been reported in some cases of HAD (39, 40). The etiology of Creutzfeldt-Jakob disease is generally considered to arise from the accumulation of plaques comprising a modified prion protein, which forms a protein polymer with a high β sheet content (41). An analogous pathogenesis for HAD, involving high molecular weight aggregates of e-gp41, can be entertained in light of the data for gp41 presented above.

Of greater significance is the observation that the pathognemonic lesion in HIV encephalopathy shares pathological, radiological, and clinical features with Binswanger's disease. In both diseases the histologic picture is diffuse demyelination of the periventricular white matter, ventricular dilation, and astrocytic gliosis (rarefaction). The computer tomography and magnetic resonance imaging patterns are nearly identical, areas of periventicular hypodensity on computer tomography, which appear as bright areas of increased intensity on T_2-weighted magnetic resonance imaging images (leukoariosis) (42, 43). Clinically, HAD is diagnosed from the acquisition of abnormalities in three areas, cognitive abilities, motor function, and social/emotional behavior (44). Similarly, Binswanger's disease is often described as the acute or gradual onset of deficits in these three areas (45). Another vascular abnormality with an identical morphology to Binswanger's disease has been reported in some cases of Alzheimer's disease exhibiting amyloid deposition (46), and a common mechanism of hypoperfusion of the deep penetrating medullary arteries from either atherosclerosis in Binswanger's disease or amyloid deposition in Alzheimer's disease has been proposed (42–44). Such hypoperfusion would be most apparent in the periventricular deep white matter, which has limited collateral perfusion. Hypoperfusion leading to ischemia has been linked to an increase in nitric-oxide synthase (47), and nitric-oxide synthase-generated NO is thought to be a major mediator of gp41 toxicity (10, 11). It is well established that free radicals generated from the ischemic processes may combine with NO to form toxic NO derivatives capable of damaging cells in a variety of ways (48). Based on the above known mechanisms and histology of encephalopathy, periventricular white matter hypoperfusion from gp41 deposition in the artery walls is another likely mechanism for HAD.

A final consideration is that HIV gp41 is currently being considered as an immunogen either in the form of injected protein, pox virus-expressing protein, or a DNA vaccine (49, 50). The observation that the gp41 ectodomain accumulates as a possibly neurotoxic aggregate in the brain suggests that the use of gp41 as an immunogen should be employed with caution. It is also possible that a peptide mapping to the loop region (residues 64–80) may be a useful immunogen for delaying or preventing the onset of HAD, in a manner analogous to the attenuation of Alzheimer disease-like pathology in a mouse model by immunization with amyloid-β peptide (51). Finally, the retroviridae used in gene therapy require the action of an envelope protein analogous to gp41 (52). The present study suggests that the solubility and stability properties of the viral envelope proteins should be taken into consideration in the design of retroviral gene therapy.

REFERENCES

1. Navia, B., Jordan, B. & Price, R. (1986) *Ann. Neurol.* **19,** 517–535
2. Price, R. W., Brew, B., Sidtis, J., Rosenblum, M., Scheck, A. C. & Cleary, P. (1988) *Science* **239,** 586–592
3. McArthur, J. C. (1987) *Medicine* (*Baltimore*) **66,** 407–437
4. Gabuzda, D. H. & Hirsch, M. S. (1987) *Ann. Intern. Med.* **107,** 383–391
5. Snider, W., Simpson, D. M., Nielsen, S., Gold, J. W., Metroka, C. E. & Posner, J. B. (1983) *Ann. Neurol.* **14,** 403–418
6. Failstich, M. E. (1986) *Int. J. Neurosci.* **30,** 249–254
7. Epstein, L. G. & Gendelman, H. E. (1993) *Ann. Neurol.* **33,** 429–436
8. Lipton, S. A. & Gendelman, H. E. (1995) *N. Engl. J. Med.* **332,** 934–940
9. Giullian, D., Vaca, K. & Noonan, C. H. (1990) *Science* **250,** 1593–1596
10. Adamson, D. C., Wildemann, B., Sasaki, M., Glass, J. D., McArthur, J. C., Chritov, V. I., Dawson, T. M. & Dawson, V. L. (1996) *Science* **274,** 1917–1921
11. Adamson, D. C., McArthur, J. C., Dawson, T. M. & Dawson, V. L. (1999) *Mol. Med.* **5,** 98–109
12. Kure, K., Llena, J. F., Lyman, W. D., Soeiro, R., Weidenheim, K. M., Hirano, H. & Dickson, D. W. (1991) *Hum. Pathol.* **22,** 700–710
13. Rostasy, K., Monti, L., Yiannoutsos, C., Kneissel, M., Bell, J., Kamper, T. L., Hedreen, J. C. & Navia, B. A. (1999) *Ann. Neurol.* **46,** 207–261
14. Lu, M., Blacklow, S. & Kim, P. S. (1995) *Nat. Struct. Biol.* **2,** 1075–1082
15. Blacklow, S., Lu, M. & Kim, P. S. (1995) *Biochemistry* **34,** 14955–14962
16. Rabinstein, M. & Shin, Y.-K. (1996) *Biochemistry* **35,** 13922–13928
17. Weissenhorn, W., Wharton, S. A., Calder, L. J., Earl, P. L., Moss, B., Aliprandis, E., Skehel, J. J. & Wiley, D. C. (1996) *EMBO J.* **15,** 1507–1514
18. Wingfield, P. T., Stahl, S. J., Kaufman, J., Zlotinick, A., Hyde, C. C. Gronenborn, A. M. & Clore, G. M. (1997) *Protein Sci.* **6,** 1653–1660
19. Caffrey, M., Cai, M., Kaufamn, J., Stahl, S. J., Wingfield, P. T., Covell, D. G., Gronenborn, A. M. & Clore, G. M. (1998) *EMBO J.* **17,** 4572–4584
20. Chan, D. C., Fass, D., Berger, J. M. & Kim, P. S. (1997) *Cell* **89,** 263–273
21. Weissenhorn, W., Dessen, A., Harrison, S. C., Skehel, J. J. & Wiley, D. C. (1997) *Nature* **387,** 426–430
22. Tan, K., Liu, J.-H., Wang, J.-H., Shen, S. & Lu, M. (1997) *Proc. Natl. Acad. Sci. U. S. A.* **94,** 12303–12308
23. Malashkevich, V. N., Chan, D. C., Chutkowski, C. T. & Kim, P. S. (1998) *Proc. Natl. Acad. Sci. U. S. A.* **95,** 9134–9139
24. Yang, Z. N., Mueser, T. C., Kaufman, J., Stahl, S. J., Wingfield, P. T. & Hyde, C. C. (1999) *J. Struct. Biol.* **126,** 131–144
25. Hainfield, J. F., Safer, D., Wall, J. S., Simon, M., Li, B. & Powell, R. D. (1994) in *Proceedings of the 52nd Annual Meeting of the Microscopic Society of America* (Bailey, G. W., and Garrat-Reed, A. D., eds.) pp. 132–133, San Francisco
26. Thomas, D., Schultz, P., Steven, A. C. & Wall, J. S. (1994) *Biol. Cell* **80,** 181–192
27. Wall, J. S., Hainfield, J. F. & Simon, M. N. (1998) in *Methods in Cell Biology* (Berrios, M., ed) Vol. 53, pp. 139–166 Academic Press, New York
28. Wiley, C. A., Schrier, R. D., Nelson, J. A., Lambert, P. W. & Oldstone, M. B. (1986) *Proc. Natl. Acad. Sci. U. S. A.* **83,** 7089–7093
29. Koenig, S., Gendelman, H. E., Oreinstein, J. M., Dal Canto, U. C., Pezeshkpour, G. H., Yungbluth., M., Janotta, F., Aksamit, A., Martin, M. A. & Fauci, A. S. (1986) *Science* **233,** 1089–1093
30. Gabuzda, D., Ho, D., de la Monte, S. M., Hirsch, M. S., Rota, T. R. & Sobel, R. A. (1986) *Ann. Neurol.* **20,** 289–295
31. Pumarola-Sune, T., Navia, B. & Cordon-Cardi, C. (1987) *Ann. Neurol.* **21,** 490–496
32. Brew, B., Rosenblum, M., Cronin, K. & Price, R. (1995) *Ann. Neurol.* **38,** 563–570
33. Glass, J. D., Fedor, H., Wesselingh, S. & McArthur, J. (1995) *Ann. Neurol.* **38,** 755–762
34. Johnson, R. T., Glass, J. D., McArthur, J. C. (1996) *Ann. Neurol.* **39,** 392–395
35. Merrill, J. E., Koyanagi, Y., Zack, J., Thomas, L., Martin, F. & Chen, I. S. Y. (1992) *J. Virol.* **66,** 2217–2225
36. Lane, T. E., Buchmeier, M. J., Watry, D. D. & Fox, H. S. (1996) *Mol. Med.* **2,** 27–37
37. Koka, P., He, K. Y., Zack, J. A., Kitchen, S., Peacock, W., Fried, I., Tran, T., Yashar, S. S. & Merrill, J. E. (1995) *J. Exp. Med.* **182,** 941–951
38. Budka, H. & Gray, F. (1993) in *Atlas of Neuropathology of HIV Infection* (Gray, F., ed) pp. 1–46, Oxford University Press, Oxford
39. Schwenk, J., Cruz-Sanchez, F., Gosztonyi, G. & Covos-Navaro, J. (1987) *Acta Neuropath.* **74,** 389–292
40. Artigas, J., Niedobitek, F., Grosse, G., Heise, W. & Gosztonyi, G. (1989) *J. Acquired Immune Defic. Syndr.* **2,** 374–381
41. Prusiner, S. (1998) *Proc. Natl. Acad. Sci. U. S. A.* **95,** 13363–13383
42. Ortiz, J. S. & Knight, P. V. (1994) *Age Ageing* **23,** 75–81
43. Osborn, A. G. (1999) in *Diagnostic Neuroradiology* (Patterson, A. S., ed) pp. 698–699, Mosby, St. Louis, MO
44. American Academy of Neurology AIDS Task Force (1991) *Neurology* **41,** 778–785
45. Wallin, A. & Blenow, K. (1993) *J. Geriatr. Psych. Neurol.* **6,** 177–188
46. Brun, A. & Englund, E. (1986) *Ann. Neurol.* **19,** 253–274
47. Heinert, G., Nye, P. C. G. & Paterson, D. J. (1999) *Acta Physiol. Scand.* **166,** 183–193
48. Cotran, R. S., Kumar, V., Robbins, S. L. & Schoen, F. J.(1994) *Pathological Basis of Disease*, Saunders, Philadelphia
49. Evans, T. G., Keefer, M. C., Weinhold, K. J., Wolff, M., Montefiori, D., Gorse, G. J., Graham, B. S., McElrath, M. J., Clements-Mann, M. L., Mulligan, M. J., Fast, P., Walker, M. C., Excler, J. L., Dubliege, A. M. & Tartaglia, J. (1999) *J. Infect. Dis.* **180,** 290–298
50. Letvin, N. L., Montefiori, D. C., Yasutomi, Y., Perry, H. C., Davies, M.-E., Lekutis, C., Alroy, M., Freed, D. C., Lord, C. I., Handt, L. K., Liu, M. A. & Shiver, J. W. (1997) *Proc. Natl. Acad. Sci. U. S. A.* **94,** 9378–9383
51. Schenk, D., Barbour, R., Dunn, W., Gordon, G., Grajeda, H., Guido, T., Hu, K., Huang, J., Johnson-Wood, K., Khan, K., Kholodenko, D., Lee, M., Liao, Z. M., Liederburg, I., Motter, R., Multer, L., Soriano, F., Shopp, G., Vasquez, N., Vanderwert, C., Walker, S., Wogulis, M., Yednok, T., Games, D. & Seubert, P. (1999) *Nature* **400,** 173–177
52. Yang, S., Delgado, R. King, S. R., Woffendin, C., Barker, C. S., Yang, Z.-Y., Xu, L., Nolan, G. P. & Nabel, G. J. (1999) *Hum. Gene Ther.* **10,** 123–132